4712 *Chem. Mater.* **2010,** *22,* 4712–4720
DOI:10.1021/cm101090p

CHEMISTRY OF MATERIALS
Article

Structure of Dealloyed $PtCu_3$ Thin Films and Catalytic Activity for Oxygen Reduction

Ruizhi Yang,[†,‡] Jennifer Leisch,[‡,§] Peter Strasser,[⊥,#] and Michael F. Toney*[,†,‡]

[†]*Stanford Institute for Materials and Energy Science, and* [‡]*Stanford Synchrotron Radiation Light Source, SLAC National Accelerator Laboratory, Menlo Park, California 94025,* [⊥]*The Electrochemical Energy, Catalysis, and Materials Science Laboratory, Department of Chemistry, Chemical Engineering Division, Technical University Berlin, 10623 Berlin, Germany, and* [#]*Department of Chemical and Biomolecular Engineering, University of Houston, Houston, Texas 77204.* [§]*Present address: National Renewable Energy Laboratory, Golden, CO 80401.*

Received April 19, 2010. Revised Manuscript Received June 28, 2010

The detailed structure and composition (surface and bulk) as well as catalytic activity for oxygen reduction of electrochemically dealloyed $PtCu_3$ thin films have been investigated. Synchrotron-based anomalous X-ray diffraction (AXRD) reveals that a Pt enriched surface region (~1.0 nm thick) and a Cu depleted interior (atomic ratio different from that of $PtCu_3$) are formed in the dealloyed film, and we directly observe a compressive lattice strain in the Pt surface region. The dealloyed $PtCu_3$ thin films show a ~2.4 fold increase in the specific oxygen reduction activity over pure Pt thin films as measured by a rotating disk electrode (RDE). Our results show that the enhanced catalytic activity of the dealloyed Pt−Cu film is primarily due to the compressive strain in the surface layer (ligand effect is very weak). We compare our results on thin films to related results on nanoparticles. These studies provide a better understanding of the structure − composition and structure − activity relationships in Pt-skeleton structures prepared by dealloying base-metal-rich alloys.

Introduction

Polymer electrolyte membrane fuel cells (PEMFC) are a promising technology for stationary and portable power applications and have the potential to reduce fossil fuel and greenhouse gas emissions by converting hydrogen and oxygen directly into electricity and water.[1] However, slow kinetics of the oxygen reduction reaction (ORR) on Pt-based catalysts at the cathode limits the efficiency of these fuel cells.[2,3] This low-efficiency cathode and the requisite high Pt loading (high cost) hinders the widespread application of PEMFCs.[2,3] This has resulted in research focused on increasing the activity of ORR catalysts[4−9] and lowering the overall Pt loading needed to efficiently perform the cathode reaction.[10−14] For designing and controlling active catalysts, a fundamental understanding of the relationship between the activity and the surface electronic structure and surface chemistry is actively being pursued.[15−20]

Alloy catalysts with Pt overlayers formed at the surface are of particular interest because of their high ORR activity and their distinct chemical and electronic properties compared to pure Pt.[18,21−28] Pt surface overlayers can

*Corresponding author: Tel.: +(650) 926 2056. E-mail: mftoney@slac.stanford.edu.

(1) Service, R. F. *Science* **2004**, *305*, 958.
(2) Adzic, R. R. In *Electrocatalysis*; Lipkowski, J., Ross, P. N., Eds.; Wiley: New York, 1998; p 197.
(3) Gasteiger, H. A.; Kocha, S. S.; Sompalli, B.; Wagner, F. T. *Appl. Catal., B* **2005**, *56*, 9.
(4) Paffet, M. T.; Beery, G. J.; Gottesfeld, S. *J. Electrochem. Soc.* **1987**, *134*, 58.
(5) Mukerjee, S.; Srinivasan, S. *J. Electroanal. Chem.* **1993**, *357*, 201.
(6) Mukerjee, S.; Srinivasan, S.; Soriaga, M. P.; McBreen, J. *J. Phys. Chem.* **1995**, *99*, 4577.
(7) Toda, T.; Igarashi, H.; Uchida, H.; Watanabe, M. *J. Electrochem. Soc.* **1999**, *146*, 3750.
(8) Paulus, U. A.; Scherer, G. G.; Wokaun, A.; Schmidt, T. J.; Stamenkovic, V.; Radmilovic, V.; Markovic, N. M.; Ross, P. N. *J. Phys. Chem. B* **2002**, *106*, 4181.
(9) Stamenkovic, V. R.; Fowler, B.; Mun, B. S.; Wang, G. F.; Ross, P. N.; Lucas, C. A.; Markovic, N. M. *Science* **2007**, *315*, 493.
(10) Zhang, J. L.; Vukmirovic, M. B.; Xu, Y.; Mavrikakis, M.; Adzic, R. R. *Angew. Chem., Int. Ed.* **2005**, *44*, 2132.
(11) Vukmirovic, M. B.; Zhang, J.; Sasaki, K.; Nilekar, A. U.; Uribe, F.; Mavrikakis, M.; Adzic, R. R. *Electrochim. Acta* **2007**, *52*, 2257.
(12) Adzic, R. R.; Zhang, J.; Sasaki, K.; Vukmirovic, M. B.; Shao, M. H.; Wang, J. X.; Nilekar, A. U.; Mavrikakis, M.; Valerio, J. A.; Uribe, F. *Top. Catal.* **2007**, *46*, 249.
(13) Zhou, W.-P.; Yang, X.; Vukmirovic, M. B.; Koel, B. E.; Jiao, J.; Peng, G.; Mavrikakis, M.; Adzic, R. R. *J. Am. Chem. Soc.* **2009**, *131*, 12755.
(14) Wang, J. X.; Inada, H.; Wu, L.; Zhu, Y.; Choi, Y. M.; Liu, P.; Zhou, W.-P.; Adzic, R. R. *J. Am. Chem. Soc.* **2009**, *131*, 17298.
(15) Mukerjee, S.; Srinivasan, S.; Soriaga, M. P.; McBreen, J. *J. Electrochem. Soc.* **1995**, *142*, 1409.
(16) Markovic, N. M.; Ross, P. N. *Surf. Sci. Rep.* **2002**, *45*, 117.
(17) Norskov, J. K.; Rossmeisl, J.; Logadottir, A.; Lindqvist, L.; Kitchin, J. R.; Bligaard, T.; Jonsson, H. *J. Phys. Chem. B* **2004**, *108*, 17886.
(18) Stamenkovic, V.; Mun, B. S.; Mayrhofer, K. J. J.; Ross, P. N.; Markovic, N. M.; Rossmeisl, J.; Greeley, J.; Norskov, J. K. *Angew. Chem., Int. Ed.* **2006**, *45*, 2897.
(19) Greeley, J.; Norskov, J. K. *J. Phys. Chem. C* **2009**, *113*, 4932.
(20) Greeley, J.; Stephens, I. E. L.; Bondarenko, A. S.; Johansson, T. P.; Hansen, H. A.; Jaramillo, T. F.; Rossemisl., J.; Chorkendorff, I.; Norskov, J. K. *Nature Chem.* **2009**, *1*, 552.
(21) Kampshoff, E.; Hahn, E.; Kern, K. *Phys. Rev. Lett.* **1994**, *73*, 704.
(22) Rodriguez, J. A. *Surf. Sci. Rep.* **1996**, *24*, 223.
(23) Rodriguez, J. A. *Prog. Surf. Sci.* **2006**, *81*, 141.
(24) Mavrikakis, M.; Hammer, B.; Nørskov, J. K. *Phys. Rev. Lett.* **1998**, *81*, 2819.
(25) Kitchin, J. R.; Nørskov, J. K.; Barteau, M. A.; Chen, J. G. *Phys. Rev. Lett.* **2004**, *93*, 156801.
(26) Kitchin, J. R.; Nørskov, J. K.; Barteau, M. A.; Chen, J. G. *J. Chem. Phys.* **2004**, *120*, 10240.
(27) Greeley, J.; Jaramillo, T. F.; Bonde, J.; Chorkendorff, I. B.; Norskov, J. K. *Nat. Mater.* **2006**, *5*, 909.

 Published on Web 07/27/2010

be formed by Pt monolayers deposited on various metal substrates[10−14] or by surface segregation from high-temperature annealing.[29−33] Another pathway to Pt surface overlayer formation is chemical/electrochemical dissolution/dealloying of non-noble elements from a bimetallic (Pt-non noble metal) alloy.[7,31−37] Depending on the dealloying method and the composition of the alloy before dealloying, the ORR activity enhancement has been attributed to an increase in Pt surface area;[34] an increase in 5d electron vacancies in the "Pt-skin" surface layer, which results in an increased O_2 adsorption and weakening of O−O bond;[7] a lowered d band center energy of the surface Pt in the "Pt-skeleton" structure relative to the Fermi level of Pt alloy surfaces, which weakens the adsorption strength between the surface Pt and spectator species;[31] and the formation of "percolated structure" with Pt-rich and Pt-poor region within individual nanoparticles.[33]

Recently, it has been shown that dealloyed Pt−Cu nanoparticle electrocatalysts formed by electrochemically dealloying Cu-rich precursors (i.e., $Pt_{25}Cu_{75}$) show uniquely high specific activities for the ORR,[38−42] resulting in a factor of 4−6 improvement over pure Pt. We have shown that these nanoparticles have a core−shell structure with a Pt-enriched shell[43,44] and proposed that compressive lattice strain was present in the Pt shell.[44] Furthermore, through a combined experimental and theoretical approach, the nanoparticle ORR activity enhancement was related to the Pt shell compressive strain and the resulting downshift and broadening of the Pt d-band that leads to a weaker oxygen bond strength.[44] However, it was not possible to accurately characterize the Pt-enriched shell structure in the dealloyed nanoparticles, because no diffraction directly from the shell could be observed, and the lattice strain in the dealloyed Pt−Cu nanoparticles was evaluated only on the basis of a two-phase core−shell model.[44] Therefore, the detailed structure of these dealloyed nanoparticles and the resulting mechanism of ORR enhancement remains incompletely understood because of the relatively nonuniform, multiphase structure, and polydispersity of the catalyst nanoparticles, which makes accurate characterization difficult.[38,41,44]

To build on our previous results and to better understand the structure−activity relationships in dealloyed Pt-alloy electrocatalysts, we report the use of uniform, single phase $PtCu_3$ ($Pt_{25}Cu_{75}$) thin films as model for accurate characterization of structure and the resulting ORR activity enhancement. Synchrotron-based anomalous X-ray diffraction (AXRD) is used to study the structure of the dealloyed Pt−Cu thin film (lattice constant and composition). Compositional inhomogeneity of the dealloyed films is observed with a Pt enriched surface region and Cu depleted interior. The composition of the Cu depleted interior is different from that of as-deposited $PtCu_3$ showing that dealloying of Cu occurs at the surface and procceds into the interior, leaving a compressively strained Pt-enriched surface region. Strain (the lattice constant/bond lengths between the metal atoms of surface layers are different from those of the parent metals) and ligand effects (heterometallic bonding interactions between the surface atoms and the substrate) are two critical factors for modification of the electronic structure and consequently chemical properties of the surface of bimetallic catalysts.[10,25,26,45] These two effects usually exist simultaneously in the first several monolayers.[10,25,26,45] In this study, because the surface region of the dealloyed Pt−Cu thin film is about 1 nm thick (4−5 monolayers), the ligand effect (active for one to three monolayers[45]) is very weak and the enhanced ORR activity of dealloyed Pt−Cu is primarily due to the compressive strain in the surface layer. We find good agreement between our measured ORR activity and Pt strain with that is predicted by theory.[44] The ORR activity enhancement factor (about 2.4 times that of Pt) in the dealloyed thin films is less than that reported in dealloyed Pt−Cu nanoparticles (about 4−6 times that of Pt) using the same precursor composition (i.e., $PtCu_3$). This activity difference is consistent with the observation that the compressive strain in the Pt surface layer of the dealloyed films is smaller than that in the Pt shell of the dealloyed nanoparticles. This is likely caused by different thickness Pt surface layers formed in the films and nanoparticles, which may be due to more dissolution of Cu in the rough or porous surface of films during dealloying as compared to small diameter nanoparticles, which may not support a porous surface.

Experimental Section

Sample Preparation. The $PtCu_3$ and pure Pt thin films were prepared by a Metallica magnetron sputter system at the

(28) Xu, Y.; Ruban, A. V.; Mavrikakis, M. *J. Am. Chem. Soc.* **2004**, *126*, 4717.
(29) Gauthier, Y. *Surf. Rev. Lett.* **1996**, *3*, 1663.
(30) Stamenkovic, V. R.; Schmidt, T. J.; Ross, P. N.; Markovic, N. M. *J. Phys. Chem. B* **2002**, *106*, 11970.
(31) Stamenkovic, V. R.; Mun, B. S.; Mayrhofer, K. J. J.; Ross, P. N.; Markovic, N. M. *J. Am. Chem. Soc.* **2006**, *128*, 8813.
(32) Stamenkovic, V. R.; Mun, B. S.; Arenz, M.; Mayrhofer, K. J. J.; Lucas, C. A.; Wang, G. F.; Ross, P. N.; Markovic, N. M. *Nat. Mater.* **2007**, *6*, 241.
(33) Chen, S.; Sheng, W.; Yabuuchi, N.; Ferreira, P. J.; Allard, L. F.; Shao-Horn, Y. *J. Phys. Chem. C* **2009**, *113*, 1109.
(34) Paffet, M. T.; Beery, G. J.; Gottesfeld, S. *J. Electrochem. Soc.* **1988**, *135*, 1431.
(35) Watanabe, M.; Tsurumi, K.; Mizukami, T.; Nakamura, T.; Stonehart, P. *J. Electrochem. Soc.* **1994**, *141*, 2659.
(36) Ding, Y.; Chen, M.; Erlebacher, J. *J. Am. Chem. Soc.* **2004**, *126*, 6876.
(37) Liu, H.; He, P.; Li, Z.; Li, J. *Nanotechnology* **2006**, 17.
(38) Koh, S.; Strasser, P. *J. Am. Chem. Soc.* **2007**, *129*, 12624.
(39) Mani, P.; Srivastava, S.; Strasser, P. *J. Phys. Chem. C* **2008**, *112*, 2770.
(40) Strasser, P. In *Handbook of Fuel Cells: Advances in Electrocatalysis, Materials, Diagnostics and Durability*; Vielstich, W., Gasteiger, H. A., Yokokawa, H., Eds.; John Wiley & Sons: Chichester, U.K., 2009; Vol. *5 & 6*, pp 30−47.
(41) Strasser, P.; Koh, S.; Greeley, J. *Phys. Chem. Chem. Phys.* **2008**, *10*, 3670.
(42) Koh, S.; Hahn, N.; Yu, C.; Strasser, P. *J. Electrochem. Soc.* **2008**, *155*, B1281.
(43) Yu, C.; Koh, S.; Leisch, J.; Toney, M. T.; Strasser, P. *Faraday Discuss.* **2008**, *140*, 283.
(44) Strasser, P.; Koh, S.; Anniyev, T.; Greeley, J.; More, K.; Yu, C.; Liu, Z.; Kaya, S.; Ogasawara, H.; Toney, M. F.; Nilsson, A. *Nat. Chem.* **2010**, *2*, 454.
(45) Schlapka, A.; Lischka, M.; Gross, A.; Kasberger, U.; Jakob, P. *Phys. Rev. Lett.* **2003**, *91*, 016101.

Stanford Nanofabrication Facility, reaching a base pressure of 1×10^{-7} Torr prior to deposition. The $PtCu_3$ and Pt sputtering targets (1.00 in. diameter, 0.125 in. thick and 99.99% pure) were obtained from Atlantic Metals & Alloys, Inc. (San Jose, CA). Both targets were sputtered using a DC power supply under 5×10^{-3} Torr Ar and cleaned by sputtering for about 1 min to remove surface impurities prior to deposition. Films were deposited onto: (1) glassy carbon (GC) disks with a diameter of 5 mm (Pine Instruments) for electrochemical measurements, which were polished to a mirror finish prior to use with 0.5 μm alumina suspension; and (2) 10 mm $\times$ 10 mm one-sided polished highly doped n-Si (100) wafers (P-doped, 4−6 Ωcm; UniversityWafer.com) for structural analysis and film thickness determination. Before deposition, the Si(100) substrates were successively degreased in acetone, ethanol and water for 15 min. Then the substrates were treated with fresh H_2SO_4/H_2O_2 solution (3:1, v/v) for 1 min to remove any trace of heavy metals and organic species. Finally the substrates were etched for 1 min in 5% HF to remove the oxide layer and thoroughly rinsed with ultrapure water. The electrical/ohmic contact, which was important for electrochemical treatments, was formed by sputtering a thin Au film on the back of the etched wafer. The thickness of both $PtCu_3$ and pure Pt films was 10 nm, which was determined using a Dektak 8 Advanced Development Profilometer (Veeco Instruments Inc.), and the estimated error is about 5%.

Electrochemical Measurements. The electrochemical measurements were conducted in a standard three-electrode electrochemical cell at room temperature. A Pt-foil was used as the counter electrode, and a Ag/AgCl (3 M Cl^-, leak-free, Cypress) reference electrode was used in a double-junction reference chamber. The potential of the Ag/AgCl reference electrode was calibrated versus the reversible hydrogen electrode (RHE). All potentials reported in this study refer to that of RHE. The electrolyte was 0.1 M $HClO_4$ solution prepared from double-distilled $HClO_4$ (70%, Sigma Aldrich) and ultrapure water (Millipore, 18.2 MΩ cm). The working electrodes were the thin film-deposited GC disks mounted in a disk-interchangeable rotating disk electrode (RDE, Pine Instruments) or the thin film-deposited Si wafers, which were mounted to a custom-made stainless steel shaft using a Teflon holder. The geometrical surface area of GC disk electrode and Si (100) electrode exposed to the electrolyte was 0.196 cm^2 and 0.503 cm^2, respectively. The working electrode potential was controlled with a potentiostat (Gamry Instruments, Reference 600). Measurements of the electro-catalytic activity of the different catalysts for Oxygen reduction reaction (ORR) were all performed on the GC disk electrodes, while the $PtCu_3$ films on Si after dealloying were used for the structure analysis because of almost zero background X-ray scattering of Si (100) substrates.

The electrolyte was deaerated by purging high-purity Ar gas into the electrolyte for at least 30 min before each electrochemical measurement. The working electrode was immersed into the Ar-saturated electrolyte under potential control and held at 0.05 V (RHE) until the measurements commenced. The initial three cyclic voltammograms were recorded between 0.05 and 1.0 V at 100 mV/s in order to monitor the early stages of the dealloying process. The dealloying was continued by 400 cyclic voltammetry (CV) potential scans between 0.05 and 1.0 V at a scan rate of 500 mV/s in Ar-saturated 0.1 M $HClO_4$ solution, which is similar to that described in ref [36]. After steady state CVs were obtained, one CV with a scan rate of 50 mV/s was collected on the dealloyed Pt−Cu on GC disk to determine the platinum electrochemical surface area (ECSA). We have dealloyed $PtCu_3$ thin films at different upper potentials (0.7−1.0 V) and these all show similar results. The platinum ECSA was determined by the mean integral charge of the hydrogen adsorption and desorption regions after double-layer correction and using 210 $\mu C\ cm^{-2}{}_{Pt}$ as the conversion factor assuming 1 H atom is adsorbed to 1 Pt atom. For the as-prepared pure Pt film on GC, the ECSA was determined in the same manner after the surface was electrochemically cleaned by sweeping the potential between 0.05 and 1.2 V (vs RHE) at 100 mV s^{-1}. The roughness factor (RF) was obtained from the ratio of ECSA to the geometric surface area (0.196 cm^2)

$$RF = ECSA/SA_{geo} \quad (1)$$

Note that the ECSA/geometrical surface area ratio of the dealloyed Pt−Cu and pure Pt films on Si are comparable to those obtained on the GC disks.

The ORR electrocatalytic activity of the dealloyed Pt−Cu and pure Pt films on the GC disks was studied with RDE using a rotator (AFMSRX, Pine Instruments). The electrolyte was purged with high-purity O_2 gas for at least 30 min to ensure O_2 saturation. Linear sweep voltammetry (LSV) measurements during oxygen reduction were performed in O_2-saturated 0.1 M $HClO_4$ by sweeping the potential from 0.05 V anodically to 1.0 V[3,9,38,46] at 20 mV s^{-1} with the electrode rotated at 400, 900, 1600, and 2500 rpm and O_2 gas purged into the solution at a rate of 1 L min^{-1} through a 2 μm fritted tube (Ace Glass). The ORR polarization curves recorded from LSV measurements on both dealloyed Pt−Cu and pure Pt at different rotation speeds all reached well-defined diffusion limiting currents (see the typical ORR polarization curves for dealloyed Pt−Cu in Figure S1 in the Supporting Information). The faradaic current density, i.e., the current due to the oxygen reduction alone, was obtained by subtracting the capacitive current (the current measured from the CV under Ar) from the ORR data and then normalized by the geometric surface area,

$$j = -(j_{ORR} - j_{capacitive,\,Ar\text{-}CV})/SA_{geo} \quad (2)$$

The kinetic current density for the ORR was derived from the Koutecky−Levich equation:

$$1/j = 1/j_k + 1/j_d = 1/j_k + 1/(B\omega^{1/2}) \quad (3)$$

where j is the measured disk current density; j_k and j_d are the kinetic and diffusion limiting current densities, respectively; B is a constant (see below); ω is the electrode rotation speed. The kinetic current density (normalized by the geometric surface area) was divided by the RF factor to obtain the ECSA normalized kinetic current density

$$j_{s,\,Pt} = j_k/RF \quad (4)$$

The ohmic resistances in the electrode contacts and electrolyte solution were assumed to be the same for dealloyed Pt−Cu and pure Pt and were not included in the corrections. The Koutecky−Levich plots for dealloyed Pt−Cu at 0.65, 0.75, 0.80, and 0.83 V ($1/j$ vs $1/\omega^{1/2}$) were linear and parallel (see Figure S1 in the Supporting Information). The experimental B values for dealloyed $PtCu_3$ is 0.153 mA $cm^{-2}\,\omega^{-1/2}$, determined from the slope of Koutecky−Levich plots, which is in good agreement with the theoretical value of 0.151 mA $cm^{-2}\,\omega^{-1/2}$ calculated for a four-electron-reduction process from the equation: $B = 0.62nFD_{O_2}{}^{2/3}v^{-1/6}C_{O_2}$, where D_{O_2} is the diffusion coefficient of O_2 ($D_{O_2} = 1.93 \times 10^{-5}$ $cm^2\ s^{-1}$), v is the kinetic viscosity of the solution ($v = 1.009 \times 10^{-2}$ $cm^2\ s^{-1}$),

(46) Paulus, U. A.; Schmidt, T. J.; Gasteiger, H. A.; Behm, R. J. *J. Electroanal. Chem.* **2001**, *495*, 134.

C_{O_2} is the concentration of O_2 dissolved in electrolyte ($C_{O_2} = 1.26 \times 10^{-3}$ mol L^{-1}),[47,48] F is the Faraday constant, and n is the apparent number of electrons transferred in the reaction. The ORR reactions on the surface of dealloyed Pt−Cu thin film are verified to proceed with $n = 4\ e^-$ reaction pathway. The specific activity was established from the ECSA normalized kinetic current density measured at 0.9 V vs RHE.

Synchrotron X-ray Diffraction and Anomalous X-ray Diffraction. Synchrotron-based X-ray diffraction (XRD) of the as-deposited $PtCu_3$ and dealloyed Pt−Cu films on Si was performed on beamline 7−2 at Stanford Synchrotron Radiation Lightsource. The synchrotron radiation source provides a high incident X-ray intensity and allows variation of the X-ray energy, which enables compositional sensitive analysis. The film samples were measured in a specular geometry with 1 milliradian analyzer collimation (Soller slit). The scattering intensity was recorded as a function of the scattering vector $Q = (4\pi \sin(2\theta/2))/\lambda$, where 2θ is the angle between the incident and diffracted X-rays and λ is the wavelength of the X-rays. The XRD data were first collected between Q of 2.0 and 6.5 $Å^{-1}$ at 8800 eV. For the anomalous X-ray diffraction (AXRD), profiles were measured in a shorter Q range (2.3−3.6 $Å^{-1}$) around the (111) peak at 22 energies between 8800 and 9160 eV, across the X-ray absorption edge of Cu at 8980 eV. The (111) peak in the XRD profile was fitted to either one or two peaks with Lorentzian function using Origin 8.0 (Origin Lab Corporation). The integrated area (A_{indiv}) of each individual fitted peak and the total integrated area (A_{total}) of (111) peak were obtained at each X-ray energy. A_{total} or A_{indiv} is directly proportional to the structure factor $|F|^2_{(111)}$ of the sample at that X-ray energy. The compositional information (molar fractions) of Pt and Cu, x_{Pt} and $y_{Cu} = 1 - x_{Pt}$, of the peaks are obtained by modeling $|F|^2_{(111),expt}$ using the relationship between the structure factor and the X-ray energy E[49]

$$|F|^2_{(111)} = |x_{Pt}[f_{Pt,111}(Q) + f'_{Pt}(E) + if''_{Pt}(E)] + x_{Cu}[f_{Cu,111}(Q) + f'_{Cu}(E) + if''_{Cu}(E)]|^2 \quad (5)$$

Here, $f(Q)$ is the atomic scattering factor, $f'(E)$ is the real part of the anomalous scattering factor, and $f''(E)$ is the imaginary part of the anomalous scattering factor, which are all known and tabulated.[50] The corresponding unit-cell parameters were deduced from the average fitted peak position obtained at each energy.

X-ray Photoelectron Spectroscopy (XPS) Analysis of the Surface Composition. Surface analysis of the films on the GC disks was performed with a SSI (Surface Science Instruments) X-ray photoelectron spectroscopy (XPS) spectrometer equipped with a hemispherical analyzer and using a monochromatized Al Kα (1486 eV) source with a 250 × 1000 μm illumination spot. The measurement parameters were as follows: 20 eV pass energy, 0.1 eV energy increments. The measurements were performed on the films on the GC disks. The spectra were corrected for the background using the Shirley approach[51] and the composition of the films was determined by measuring the ratio of Pt4f to Cu2p intensities (integrated peak area) normalized by their respective sensitivity factors.[52] The probing depth (about 1.6 nm) is obtained from the inelastic mean free path of Pt4f and Cu2p estimated from TPP-2 M equation described by Tanuma et al.[53]

Surface Morphology. The morphology of films before and after dealloying was studied using a FEI XL30 Sirion scanning electron microscope (SEM).

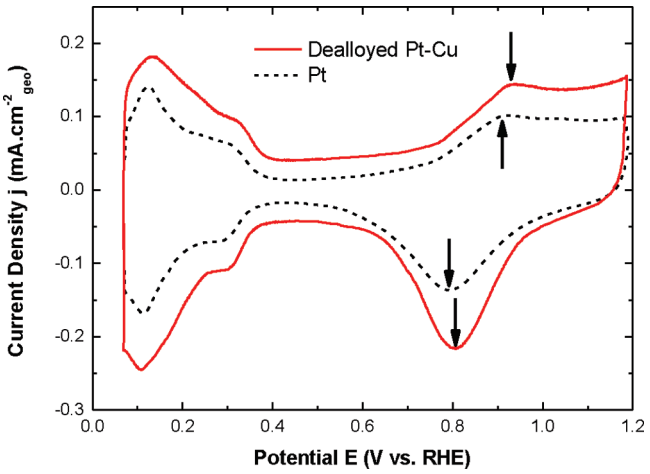

Figure 1. Cyclic voltammetry of dealloyed Pt−Cu and pure Pt films. Experiments were conducted in Ar-saturated 0.1 M $HClO_4$ at 298 K with a sweep rate of 50 mV/s. The positions of the peak anodic current densities due to adsorption of oxygenated species/oxidation of surface atoms as well as the peak cathodic current densities due to desorption of oxygenated species/reduction of surface oxide are marked with arrows.

Results and Discussion

Cyclic Voltammetry and Catalytic Activity. Cyclic voltammetry (CV) of dealloyed Pt−Cu and pure Pt films on GC disks are shown in Figure 1. The CV of dealloyed Pt−Cu resembles that of pure Pt, but shows an increased interfacial capacitance seen by the difference in capacitive current in the double layer region (0.4−0.7 V). The ECSAs of dealloyed Pt−Cu and pure Pt were determined from the charge of H adsorption/desorption and are given in Table 1. The ECSA of dealloyed Pt−Cu (0.528 cm^2) is about 1.5 times that of pure Pt (0.350 cm^2). The roughness factors (ratio of ECSA to geometric surface area) for dealloyed Pt−Cu and pure Pt are 2.7 and 1.8, respectively, which shows that a rougher surface is formed on dealloyed Pt−Cu films due to leaching of Cu and explains why dealloyed Pt−Cu films show an increased interfacial capacitance (see Figure 1). SEM image of the Pt−Cu film after dealloying in Figure S2 in the Supporting Information shows the rougher surface containing cracks and voids, which is consistent with the roughness factor measured by CV. There is also likely some roughness or porosity that is below the resolution of the SEM. This is in agreement with the results of acid treated non-noble metal (Fe, Co, Ni)-rich Pt alloy thin films in 0.1 M $HClO_4$[6] and that of a Pt−Fe thin film subjected to potential cycling in 0.1 M HF solution.[54] In the potential

(47) Markovic, N. M.; Gasteiger, H. A.; Ross, P. N. *J. Phys. Chem.* **1995**, *99*, 3411.
(48) Lide, D. R. *CRC Handbook of Chemistry and Physics*; CRC Press: Boca Raton, FL, 1995.
(49) DeGraef, M.; McHenry, M. E. *Structure of Materials: An Introduction to Crystallography, Diffraction, and Symmetry*; Cambridge University Press: Cambridge, U.K., 2007.
(50) Pecharsky, V.; Zavalij, P. Y. *Fundamentals of Powder Diffraction and Structural Characterization of Materials*; Springer: New York, 2003.
(51) Shirley, D. A. *Phys. Rev. B* **1972**, *5*, 4709.
(52) Briggs, D. Seah, M. P. *Practical Surface Analysis*; Wiley Interscience: New York, 1990.
(53) Tanuma, S.; Powell, C. J.; Penn, D. R. *Surf. Interface Anal.* **1993**, *21*, 165.
(54) Wakisaka, M.; Suzuki, H.; Mitsui, S.; Uchida, H.; Watanabe, M. *J. Phys. Chem. C* **2008**, *112*, 2750.

Table 1. Electrochemical Surface Areas, Roughness Factors, Faradaic Current Densities, Kinetic Current Densities and Specific Activities of Pt and Dealloyed Pt−Cu[a]

sample	electro-chemical surface area (ECSA, cm^2_{Pt})	roughness factor (RF, cm^2_{pt}/cm^2_{geo})	absolute activity at 0.9 V (mA)	capacitive current (mA)[b]	faradaic current density $j_{(0.9\ V)}$ (mA/cm^2_{geo})	diffusion-limiting current density j_D (mA/cm^2_{geo})	kinetic current density $j_{k\ (0.9\ V)}$ (mA/cm^2_{geo})[c]	specific activity $j_{s\ (0.9\ V)}$ (mA/cm^2_{Pt})[d]
Pt	0.350	1.8	0.2622	0.001567	1.330	6.04	1.706	0.95
dealloyed Pt−Cu	0.528	2.7	0.6026	0.004115	3.053	6.12	6.092	2.26

[a] ORR activities were obtained in O_2-saturated 0.1 M $HClO_4$ at 1600 rpm at a scan rate of 20 mV/s at room temperature. [b] Measured from CV under Ar at a scan rate of 20 mV/s. [c] $j_k = \frac{1}{\frac{1}{j} - \frac{1}{j_D}}$. [d] $j_s = j_k/RF$.

region of 0.7−1.2 V (see Figure 1), a positive shift in the peak potential on dealloyed Pt−Cu relative to pure Pt is observed (arrows), which suggests a delayed oxide formation/adsorption of oxygenated species[9,16,30,55−60]

The oxygen reduction activities of the dealloyed Pt−Cu and pure Pt films are shown in Figure 2a. The currents shown were measured at 1600 rpm and normalized by the geometric area. There is a positive shift of 36 mV in the half-wave potential of dealloyed Pt−Cu as compared to pure Pt, which shows that dealloyed Pt−Cu is more active than pure Pt. The diffusion-current-corrected Tafel plots of specific ORR activity of the samples are shown in Figure 2b. At 0.9 V, the specific activity of dealloyed Pt−Cu is 2.26 mA cm^{-2}_{Pt}, which is about 2.4 times that of Pt (0.95 mA cm^{-2}_{Pt}, Table 1). It should be noted that the specific activity of the sputtered pure Pt thin film at 0.9 V is in good agreement with the specific activity of polycrystalline Pt at the same potential reported elsewhere.[30]

Structure of Thin Films and Its Correlation with ORR Activity. X-ray diffraction profiles of the as-deposited $PtCu_3$, dealloyed Pt−Cu and as-deposited Pt films on Si(100) are shown in Figure 3. Both the as-deposited $PtCu_3$ and Pt films show single phase face centered cubic (FCC) structures. The average lattice constants obtained from the best fitting for the as-deposited $PtCu_3$ and Pt film are 3.716 and 3.921 Å, respectively, which are in close agreement with those reported for bulk materials.[60] In contrast, the diffraction peaks of dealloyed Pt−Cu shift toward lower Q and are broader compared to the as-deposited $PtCu_3$, showing that Cu is leached from $PtCu_3$ alloy and that the microstructure becomes more disordered with a smaller grain size. In addition, the dealloyed diffraction peaks are asymmetric, indicating the formation of a nonuniform structure after dealloying, which will be discussed in detail below. Note that the X-ray diffraction peaks obtained on the dealloyed Pt−Cu on glassy carbon are in good agreement with those obtained on Si(100) although there are peak overlaps between dealloyed Pt−Cu and the glassy carbon (see Figure S3 in the Supporting Information). This shows

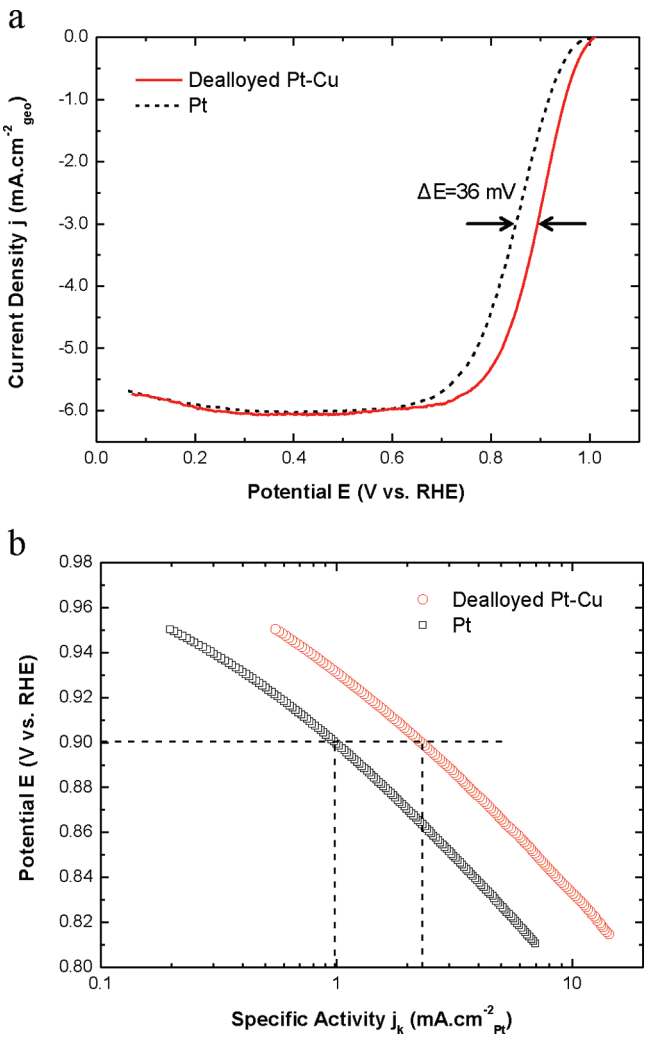

Figure 2. (a) Oxygen reduction currents measured on dealloyed Pt−Cu and pure Pt films at a rotation speed of 1600 rpm. Experiments were conducted in O_2-saturated 0.1 M $HClO_4$ at 298 K with a sweep rate of 20 mV/s. Arrows indicate the values of half-wave potentials. (b) Pt surface normalized ORR activities of dealloyed Pt−Cu and pure Pt in (a).

that the structure of the dealloyed Pt−Cu on Si is the same as that on glassy carbon, permitting a correlation between structure (films on Si) and activity (films on GC).

To determine the structure (e.g., lattice constant and composition) of the dealloyed Pt−Cu thin film, anomalous X-ray diffraction (AXRD) was performed in the energy range of the Cu absorption K edge (8980 eV). AXRD profiles of the as-deposited $PtCu_3$ and dealloyed Pt−Cu at several energies are shown in Figures 4 a and b. As the X-ray energy approaches the Cu edge, a decrease in

(55) Mukerjee, S.; McBreen, J. *J. Electroanal. Chem.* **1998**, *448*, 163.
(56) Murthi, V. S.; Craig Urin, R.; Mukerjee, S. *J. Phys. Chem. B* **2004**, *108*, 11011.
(57) Markovic, N. M.; Schmidt, T. J.; Stamenkovic, V. R.; Ross, P. N. *Fuel cells* **2001**, *1*, 105.
(58) Antoine, O.; Bultel, Y.; Durand, R. *J. Electroanal. Chem.* **2001**, *499*, 85.
(59) Wang, J. X.; Markovic, N. M.; Adzic, R. R. *J.Phys.Chem. B* **2004**, *108*, 4127.
(60) Villars, P.; Calvert, L. D. *Pearson's Handbook of Crystallographic Data for Intermetallic Phases*; ASM International: Materials Park, OH, 1991.

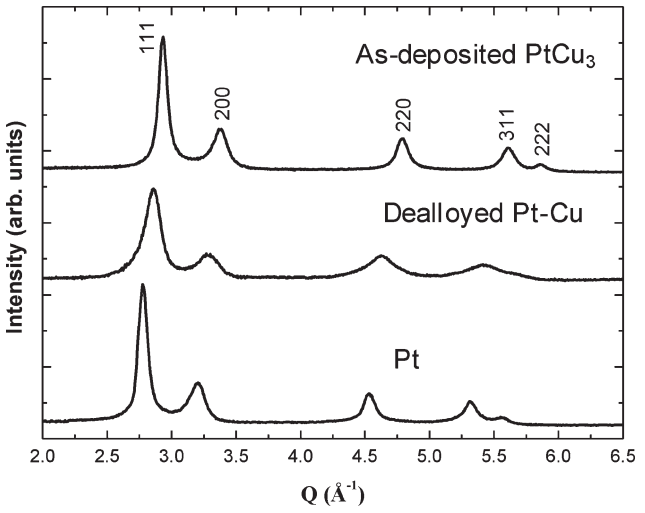

Figure 3. X-ray diffraction profiles of as-deposited $PtCu_3$, dealloyed Pt−Cu, and as-deposited Pt film samples on Si(100).

scattering intensities of the (111) and (200) Bragg reflections is observed. This intensity decrease is related to the drop in scattering power of Cu near the edge and allows the Cu content of the scattering phase to be accurately determined. Figure 4 c and d show the fitting of typical profiles of the as-deposited $PtCu_3$ and the dealloyed Pt−Cu, respectively. The (111) reflection of as-deposited $PtCu_3$ can be fitted to one peak. However, the (111) reflection of dealloyed Pt−Cu is asymmetric and must be fitted to two peaks, which we identify as peak 1 and peak 2 in Figure.4d. The energy dependence of the (111) integrated intensity for the as-deposited $PtCu_3$ and dealloyed Pt−Cu is shown in panels a and b in Figure 5, respectively. As the Cu edge energy is approached, the integrated intensity for the as-deposited $PtCu_3$ drops as expected, as does that for peak 2 (higher Q) of the dealloyed Pt−Cu. In striking contrast, the integrated intensity for peak 1 of the dealloyed Pt−Cu does not decrease near the Cu absorption edge. This shows that the phase causing peak 1 is free of Cu to within our measurement ability of about 4%. The XPS data show that the near-surface Cu composition of the dealloyed Pt−Cu is 9% (Table 2, further details will be discussed below). Thus from the XPS and AXRD, we conclude that peak 1 corresponds to a nearly pure Pt surface layer and peak 2 corresponds to the interior region of dealloyed Pt−Cu still containing Cu.

The (111) diffraction peak for the Pt surface layer (peak 1) is centered at $Q = 2.792 \pm 0.007$ Å^{-1} (average position from AXRD). The corresponding lattice constant ($a_{surface}$) is 3.897 ± 0.007 Å, which is smaller than that of pure Pt ($a_{Pt} = 3.923$ Å^{-1}). The surface region thus has a compressive strain ($S = ((a_{surface} - a_{Pt})/a_{Pt}) \times 100)$) of $-0.66 \pm 0.18\%$ with respect to pure Pt. It has to be noted that if we fit peak 1 with a lattice constant of pure Pt, we cannot fit the complete spectra adequately.

The average chemical compositions of the as-deposited $PtCu_3$, the dealloyed Pt−Cu (overall, i.e. peak 1 + peak 2) and the interior region of the dealloyed Pt−Cu films (peak 2) are determined from the relationship between the integrated intensity and X-ray energy based on eq 5. Figures 5c−e show the fits from eq 5 for the (111) integrated intensity of the as-deposited $PtCu_3$, the dealloyed Pt−Cu (overall, i.e, peak 1+ peak 2) and the interior region of the dealloyed Pt−Cu films (peak 2) as a function of energy. The resulting compositions are listed in Table 2. For the as-deposited $PtCu_3$ ($Pt_{25}Cu_{75}$), the best fit gives a composition of $Pt_{26}Cu_{74}$. This agrees with the nominal composition well within the estimated error of 4%, giving an internal check of our technique. As further evidence of a uniformly alloyed initial material, the surface composition measured from XPS for the as-deposited is $Pt_{25}Cu_{75}$ (see Table 2), showing that the as-deposited $PtCu_3$ film is uniformly alloyed. As discussed above, the dealloyed Pt−Cu consists of a Pt enriched surface layer and Cu depleted alloy interior. The difference between the surface composition ($Pt_{91}Cu_9$) as determined by XPS (probing depth of 1.6 nm), the interior composition ($Pt_{59}Cu_{41}$) and the overall composition ($Pt_{68}Cu_{32}$) as determined by AXRD shows the vertical inhomogeneity of the dealloyed Pt−Cu film. Importantly, the interior composition of dealloyed Pt−Cu ($Pt_{59}Cu_{41}$) is different from that of the sample before dealloying ($Pt_{25}Cu_{75}$), which is different from what was proposed in nanoparticles, where the core (i.e., interior) composition of the dealloyed Pt−Cu nanoparticles was assumed to be the same as that of the precursor.[44] This shows that dealloying of Cu also occurs in the interior region, and not only in the near surface region, which is consistent with the dealloying process on flat surfaces obtained from the kinetic Monte Carlo simulation of the Ag−Au dealloying reported by Erlebacher et al.[61,62]

The dealloying of $PtCu_3$ is depicted schematically in Figure 6. Both the as-deposited $PtCu_3$ and dealloyed Pt−Cu have FCC crystal structure as shown by the initial XRD profiles (Figure 3). The as-deposited $PtCu_3$ thin film is uniform, well alloyed and single phase. After dealloying, most Cu is removed from the surface and partially from the interior, leaving a nearly pure Pt enriched surface layer with compressive strain of 0.66 ± 0.18% (relative to Pt) which covers a Cu depleted interior ($Pt_{59}Cu_{41}$). This is similar to "Pt-skeleton" structure proposed by Stamenkovic et al.[31] It is worth mentioning that the lattice parameter of the interior of the dealloyed Pt−Cu (peak 2) estimated using Vegard's rule ($a = 3.923x + 3.615(1-x)$ for Pt_xCu_{1-x}, the interior composition is $Pt_{59}Cu_{41}$) is 3.797 Å, which is in excellent agreement with the lattice parameter of 3.802 Å obtained from the peak position (peak 2) by AXRD. From the AXRD derived surface and interior compositions and lattice parameters, the thickness of the Pt surface layer in the dealloyed Pt−Cu can be estimated (see the Supporting Information for the details). The thickness of the Pt surface layer of dealloyed film is about 1.0 nm. The estimated probing depth for the XPS measurement at photon energy of 1486 eV (Al K_α) is 1.6 nm,[53] where only 9% Cu is detected (Table 2), which is in reasonable agreement with our estimate of the Pt surface region for the dealloyed film.

(61) Erlebacher, J.; Aziz, M. J.; Karma, A.; Dimitrov, N.; Sieradzki, K. *Nature* **2001**, *410*, 450.
(62) Erlebacher, J. *J. Electrochem. Soc.* **2004**, *151*, C614.

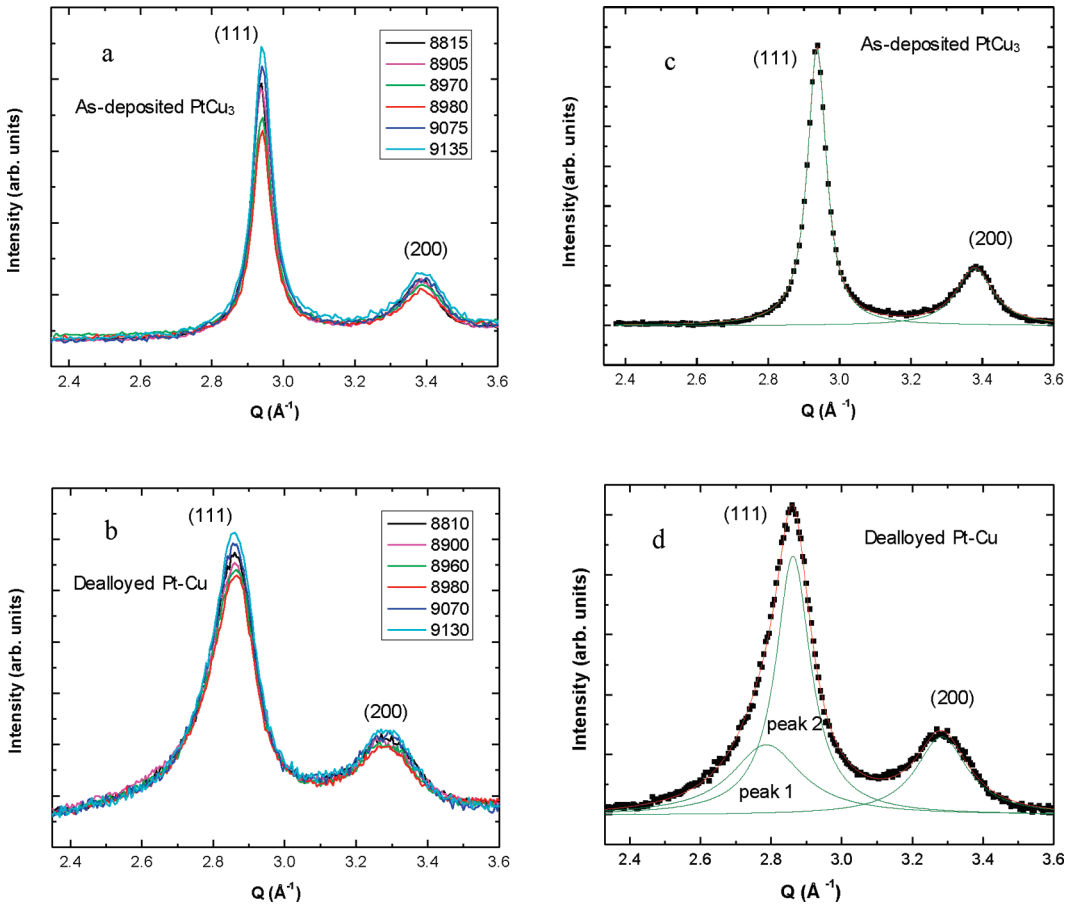

Figure 4. Anomalous X-ray diffraction (AXRD) profiles of the (a) as-deposited $PtCu_3$ and (b) dealloyed Pt−Cu as a function of the scattering vector Q at indicated energies. Fitting (Lorentz function) of a typical XRD profile of the (c) as-deposited $PtCu_3$ taken at 8815 eV and the (d) dealloyed Pt−Cu taken at 8810 eV.

It has been reported by Fusy et al. that five monolayers of Pt grown on Cu (111) gave a compressive strain of −1.2 to approximately −1.9% according to reflection high energy electron diffraction.[63] In our study, 4−5 monolayers Pt (about 1.0 nm) on dealloyed Pt−Cu gives a compressive strain of −0.66 ± 0.18%, which is reasonably consistent with the results reported by Fusy et al. considering the substrates are different.

The reaction driving force/activity of dealloyed Pt−Cu relative to pure Pt can be calculated as $A = kT\ln(j_{Pt-Cu}/j_{Pt})$, where $j_{Pt-Cu}/j_{Pt} = 2.4 \pm 0.2$, which is the ratio of specific activity of dealloyed Pt−Cu relative to Pt at 0.9 V vs RHE, $T = 298$ K. We find that the activity $A = 0.023 \pm 0.002$ eV. This is in close agreement with the value of about 0.028 eV obtained from the linear relationship between the lattice strain and the oxygen adsorption energy shown by the density functional theory (DFT) studies of Marvrikakis et al.[24] as well as the linear relationship between the activity A and the oxygen adsorption energy on the left side of the volcano-shaped plot shown by the DFT studies of Norskov et al.[18]

It was shown that compressive strain in the Pt surface layer modifies the d-band structure of the Pt atoms (i.e., broadens the d band) and lowers valence band center relative to the Fermi level, resulting in a decrease in the adsorption energy of reactive intermediates and thus an increase in the catalytic activity of the Pt surface.[24,25,44,45,64−66] However, it has been difficult to clearly separate the strain and ligand effects in the first several monolayers because these usually occur together.[10,25,26] It has been reported that the ligand effect in the Pt surface layer is negligible beyond three Pt monolayers as the electronic influence of underlying substrates/elements decays quickly with Pt layer thickness.[45] Thus, the ligand effect is very weak in our dealloyed Pt−Cu film, because the Pt surface layer consists of 4−5 Pt monolayers. The ORR activity enhancement in the dealloyed Pt−Cu thin film can then be primarily attributed to the compressive strain in the Pt surface layer, which modifies the electronic structure of Pt surface layer[24,25,45,64−66] and results in the lower adsorption energy of surface Pt toward oxygenated species. This is consistent with the observation that the peak potential of adsorption of oxygenated species/oxide formation is positively shifted on dealloyed Pt−Cu relative to pure Pt (Figure 1), an indication of delayed oxide formation/adsorption of oxygenated species.

(63) Fusy, J.; Meneaucourt, J.; Alnot, M.; Huguet, C.; Ehrhardt, J. J. *Appl. Surf. Sci.* **1996**, *93*, 211.
(64) Xu, Y.; Ruban, A. V.; Mavrikakis, M. *J. Am. Chem. Soc.* **2004**, *126*, 4717.
(65) Grabow, L.; Xu, Y.; Mavrikakis, M. *Phys. Chem. Chem. Phys.* **2006**, *8*, 3369.
(66) Gsell, M.; Jakob, P.; Menzel, D. *Science* **1998**, *280*, 717.

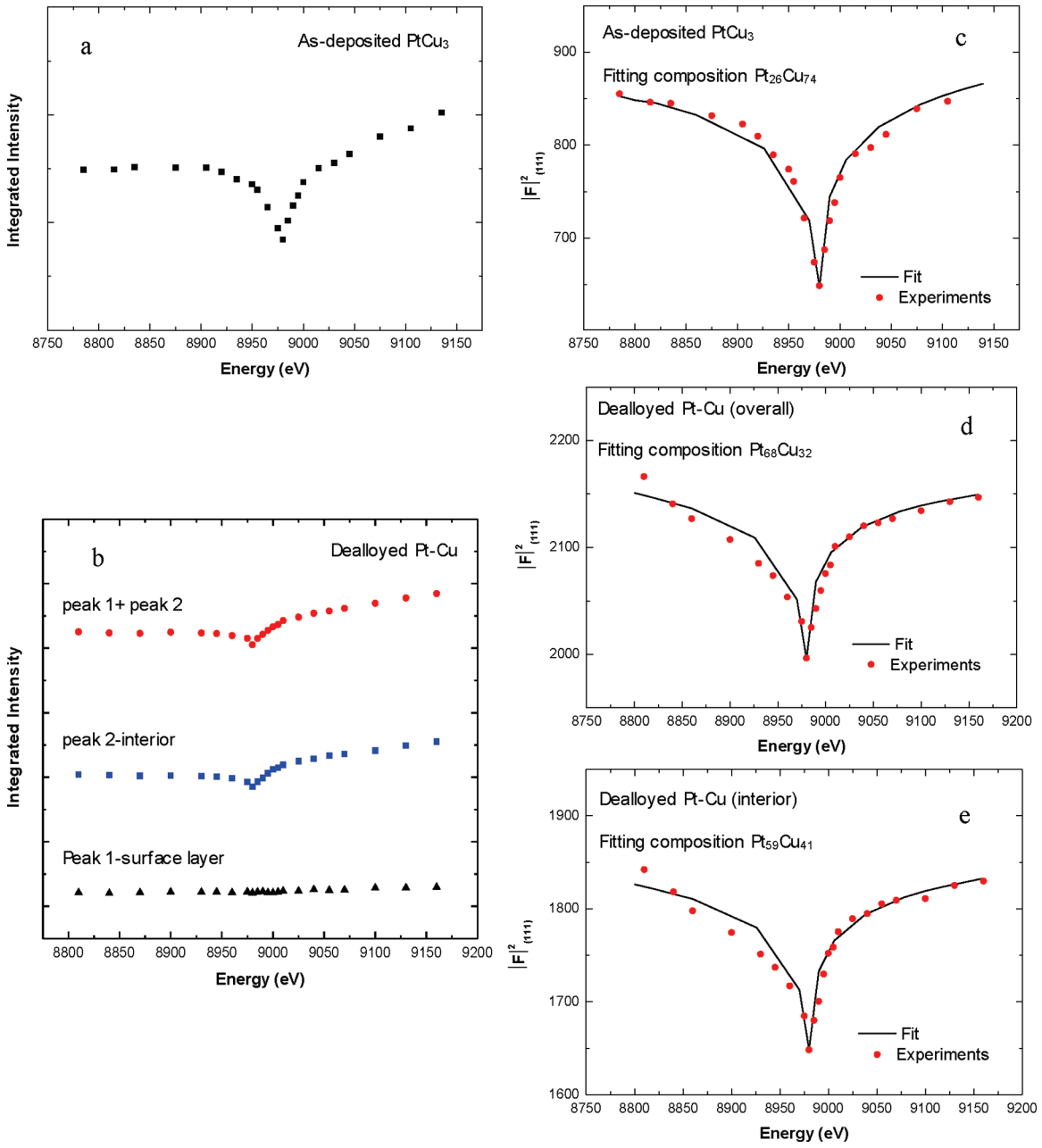

Figure 5. Integrated intensity of (111) reflection for the (a) as-deposited $PtCu_3$ and (b) dealloyed Pt−Cu as a function of X-ray energy. The fitting from the calculation (eq 5) for the integrated intensity of (111) reflection of the (c) as-deposited $PtCu_3$, (d) dealloyed Pt−Cu, and (e) interior of dealloyed Pt−Cu as a function of X-ray energy.

Table 2. Bulk Composition (from AXRD), Surface Composition (from XPS) and the Lattice Constants for the As-Deposited $PtCu_3$ and Dealloyed Pt−Cu Thin Film

sample	as-deposited $PtCu_3$	dealloyed Pt−Cu (overall)	dealloyed Pt−Cu (interior)	dealloyed Pt−Cu (surface layer)
bulk composition (AXRD)	$Pt_{26}Cu_{74}$	$Pt_{68}Cu_{32}$	$Pt_{59}Cu_{41}$	Pt
surface composition (XPS)	$Pt_{25}Cu_{75}$	$Pt_{91}Cu_9$		
lattice parameter (Å)	3.716		3.802	3.897

We can combine our results on electrochemically dealloyed Pt−Cu thin films from a Cu rich $PtCu_3$ precursor with those of Stamenkovic et al.[31] on dealloyed polycrystalline Pt_3Co and PtCo, where Co is chemically dissolved while the surfaces were exposed to acid. From this, we find that the richer the alloy is in base metal, the more the base metal is dissolved from the alloy whether the dealloying is performed chemically or electrochemically.

Finally, we note that the detailed structure of the dealloyed Pt−Cu thin film (lattice constant and composition) can be accessed because of the uniform and single-phase structure of thin films as compared with the relatively nonuniform, multiphase structure and large polydispersity in the Pt−Cu nanoparticles. Recall that in the latter, the lattice constant is estimated based on a two phase core−shell model where the average lattice constant and

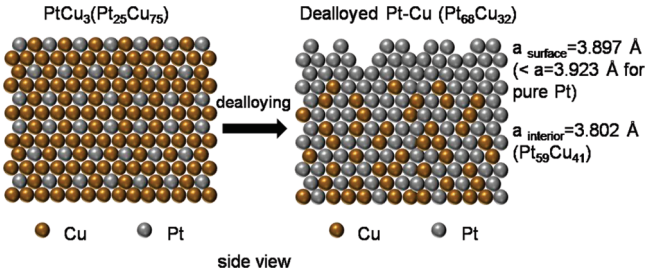

Figure 6. Schematic of the dealloying of $PtCu_3$ film.

composition must be known. Consequently, the strain is directly and more accurately determined in the dealloyed thin film. The thickness of the Pt-enriched surface layer of the dealloyed Pt−Cu thin film (about 1.0 nm) is larger than that of dealloyed Pt−Cu nanoparticles (about 0.4−0.6 nm).[43,44] Relative to the nanoparticles, this thicker layer relaxes more and is thus less compressively strained;[45] this results in the lower ORR activity enhancement (about 2.4 times Pt) compared to that of dealloyed nanoparticles (about 4−6 times Pt).[38] Although we are unsure of the exact mechanism resulting in the formation of thicker Pt surface layer in the dealloyed thin films, we speculate that this could be due to the fact that more Cu is dissolved in the surface layers because the surface of films becomes rough or porous during the dealloying and small diameter nanoparticles may not support the porous surface (Indeed, no surface roughing is observed in dealloyed Pt−Cu nanoparticles[38]). We cannot, however, rule out other possibilities.

Conclusions

This work presents an accurate characterization of a Pt-skeleton structure prepared by dealloying base metal rich alloy thin films and a detailed understanding of the structure and composition relationships using AXRD. Our results show that dealloyed Pt−Cu thin films consist of a Pt enriched surface layer and Cu depleted interior and that the Pt surface layer is compressively strained. This surface layer compressive strain dominates the ORR activity enhancement in the dealloyed Pt−Cu film, which is consistent with the DFT studies of Norskov et al.[18] and Mavrikakis et al.[24] We find that the compressive strain (and hence ORR activity) in the Pt surface layer is smaller in the films compared to the similarly dealloyed nanoparticles, which likely results from the thicker Pt rich layer on the films.

Acknowledgment. This work is supported by the Department of Energy, Office of Basic Energy Sciences, Division of Materials Sciences and Engineering, under Contract DE-AC02-76SF00515 and under the auspices of the grant LAB04-20. Portions of this research were carried out at the Stanford Synchrotron Radiation Light Source, a national user facility operated by Stanford University on behalf of the U.S Department of Energy, Office of Basic Energy Sciences. Thin film preparation and lab-source characterization were carried out at Stanford Nanofabrication Facility and Stanford Nanocharacterization Laboratory, respectively. We thank Seungsae Hong at Department of Applied Physics, Stanford University, for the assistance in SEM measurement.

Supporting Information Available: (1) The polarization curves for the ORR on dealloyed Pt−Cu, SEM images of Pt−Cu thin film before and after dealloying and X-ray diffraction profiles of glassy carbon disk, and of dealloyed Pt−Cu thin film on Si(100) and glassy carbon disk (Figure S1 to S3, respectively); (2) an explanation of the method used to estimate the thickness of Pt enriched surface layer in the dealloyed Pt−Cu films (PDF). This material is available free of charge via the Internet at http://pubs.acs.org/.